Desalination and Water Treatment
www.deswater.com

doi: 10.5004/dwt.2019.23334

138 (2019) 379–388
January

Magnetic core layered double hydroxide over halloysite as a robust adsorbent for the treatment of dye-contaminated wastewater: a clean approach for industrial applications

Shappur Vahidhabanu[a,b,*], Adeogun Abideen Idowu[a,c], B. Ramesh Babu[a,b,*]

[a]*CSIR-Central Electro Chemical Research Institute, Pollution Control Division, Karaikudi 630003, Tamil Nadu, India, Tel. +91 4565 241441; Fax: +91 4565 227779; emails: vahishappur@gmail.com (S. Vahidhabanu), brbabu@cecri.res.in (B.R. Babu)*
[b]*Academy of Scientific and Innovative Research (AcSIR), Ghaziabad-201002, India*
[c]*Chemistry Department, Federal University of Agriculture, Abeokuta, Nigeria, email: adeogunai@funaab.edu.ng*

Received 3 July 2018; Accepted 21 October 2018

ABSTRACT

A three-component nanocomposite containing halloysites-coated, Fe_3O_4 magnetic core and layered double hydroxide (HNT@Fe_3O_4@LDH) (HFL) was successfully synthesized via a layer-by-layer deposition method followed by an in-situ growth method. The synthesized nanocomposite was characterized using X-ray diffraction and Fourier-transform infrared to confirm the nanocomposite formation. The structure of HFL was approved by scanning electron microscopy and high-resolution transmission electron microscope. The HFL nanocomposite was applied for the adsorptive removal of Congo red (CR) dye from aqueous medium. The kinetic and isotherm studies were also performed using different models. Kinetic results were best described by the pseudo-first-order model with $R^2 > 0.9$ and the process could be described while mass transfer dominated. The nanocomposite demonstrated favourable adsorption properties towards CR dye with maximum adsorption capacity (Q_{max}) of 225.11 mgg^{-1}, separation factor (R_L) of 0.14 and theoretical saturation capacity (Q_s), of 172.85 mg g^{-1}. The maximum adsorption energies (E = 0.40 kJ mol^{-1}) showed that the process was physisorption in nature. The isotherm models fitted in the order of Dubinin–Radushkevich > Langmuir > Temkin > Freundlich isotherm. The adsorptive removal of CR dye by HFL compared favourably well with other adsorbents in the same category with better regeneration.

Keywords: Halloysite composites; Layer-by-layer deposition process; Dye; Congo red; Wastewater treatment

1. Introduction

Industries such as paper, textile, plastics, cosmetic, rubber, leather, pesticide, food, pharmaceutical, etc. discharge large amount of wastewater-containing toxic organic dyes which can create health problems, even at low concentrations [1,2]. Many of these dyes are non-biodegradable with high toxicity, carcinogenicity, and teratogenicity, and when allowed to enter food chain, they pose threat to living organisms [3], consequently these highly coloured effluents required proper treatments before their discharge into receiving water in the environment.

Wide range of techniques has been developed for wastewater treatments. The techniques include coagulation, flocculation, chemical oxidation, membrane filtration, catalytic degradation, adsorption, and photochemical degradation [4–10]. Among these methods, adsorption is considered as one of the best methods due to its environmental compatibility, cost-effectiveness, ease of operation, and high efficiency [11–13].

Activated carbon is mostly used in industrial wastewater treatment systems due to its large specific surface area [9]. However, its feasibility in large-scale wastewater treatment

* Corresponding authors.

is limited due to its expensiveness and other factors. Hence, a continue effort for inexpensive alternative adsorbents with sound adsorption efficiencies and recyclability is desirable. Recent development in the field of nanotechnology has led to the synthesis of many nanocomposites that are highly efficient in wastewater treatment. The synthesis of clay polymer and ZnO–clay nanocomposite, which are highly efficient adsorbents for remediation of dye-contaminated wastewater, has been recently reported. [9]. Efforts have now shifted to incorporation magnetic components onto micro/nano-sized hierarchical structures for potential use as adsorbent [13,14]. This is to harness their large specific surface area and improved mechanical properties, above all to enhance recovery through the application of an external magnetic field. Halloysite nanotube (HNT), a clay mineral with one-dimensional tubular structure is abundant in nature. Its high adsorption capacity, tuneable surface chemistry, adequate hydroxyl groups, and environmental friendly properties have fascinated material scientists [15]. HNT has been used extensively used for the removal of pollutants [16–18] and oil entrapment [19]. Layered double hydroxides (LDH), also known as anionic clays, are known for their biocompatibility and non-toxicity when compared with other inorganic compounds in the same category. They have been widely applied in adsorption [20], electrochemical, and immobilization applications [21].

The study aimed at developing a low-cost, environmental friendly adsorbent with improved adsorption capacity, ease of recovery, as well as better thermal and mechanical properties. Hence, a layer-by-layer technique was used for the facile synthesis of Fe_3O_4@HNT@LDH. The synthesized nanocomposite was used for the removal of Congo red (CR) dye. The effects of various operating parameters on the adsorption process were also investigated. Data obtained were subject to kinetic and isotherm analysis.

2. Experiments

2.1. Synthesis of HNT-Fe_3O_4

Halloysite-magnetite (HNT-Fe_3O_4) material was synthesized via co-precipitation technique. Briefly, 1 g of HNT was dispersed in 180 mL of solution comprising 1 mmol $FeCl_2$ $4H_2O$ and 2 mmol $FeCl_3$ $6H_2O$. The mixture was sonicated for 25 min and further stirred at 60°C for 30 min under N_2 atmosphere. This was followed by addition of 20 mL of ammonia solution while the pH was maintained between 9 and 11. The suspension was allowed to age 70°C for 4 h, followed by centrifugation and washing with distilled water. The solid residue was dried overnight in a vacuum oven at 60°C.

2.2. Synthesis of HNT@Fe_3O_4@AlOOH

AlOOH primer sol was obtained by hydrolysis of γ-AlOOH (boehmite) according to the method of Granados-Correa and Jimenez-Becerril [22]. A dispersion containing 5.8 g of boehmite in 107 mL deionized (DI) water was prepared, stirred at 85°C for 1 h, while nitric acid (9.5 mL, 1.0 M) was added dropwise with continuous stirring for a period of 6 h. The resulting AlOOH was cooled to room temperature, after which HNT–Fe_3O_4 was dispersed in it under constant agitation for 1 h. The product was cooled to room temperature, washed recurrently with C_2H_5OH, followed by drying for 30 min in air (washing and drying at least five times). The subsequent material, HNTs@Fe_3O_4@AlOOH, was vacuum dried at 35°C for 24 h.

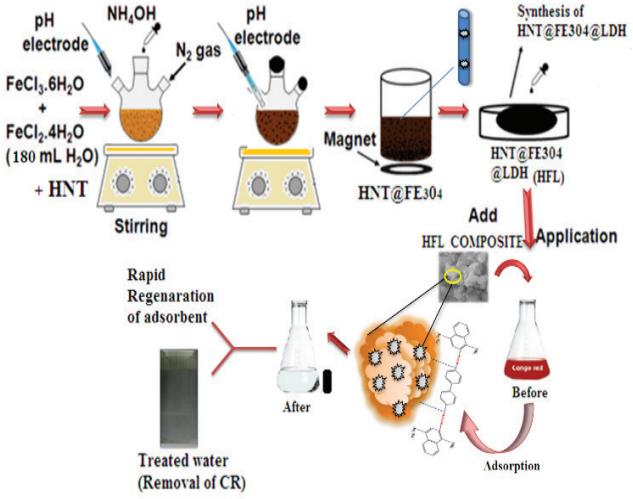

Fig. 1. Synthesis and application of HNT@Fe_3O_4@LDH for CR dye removal.

2.3. Synthesis of HNT@Fe_3O_4@LDH

Synthesis of HNT@Fe_3O_4@LDH was accomplished by dispersing 0.3 g of HNT@Fe_3O_4@AlOOH into a solution having 0.005 mol magnesium nitrate and 0.04 mol urea in 200 mL of DI water. This was then transferred into autoclave and heated at 80°C for 48 h. After that, it was cooled at room temperature and HNT@Fe_3O_4@LDH was centrifuged and washed frequently with C_2H_5OH and dried at room temperature. The synthesis and application of the HNT@Fe_3O_4@LDH are as summarized in Fig. 1.

3. Characterization

X-ray diffraction (XRD) technique was obtained with a PAN Analytical XPert PRO XRD and Cu Ka radiation (λ = 1.5418 Å) was used to make out the crystal structure of prepared microspheres. Fourier-transform infrared (FTIR) spectra were recorded from 400 to 4,000 cm^{-1} in TENSOR 27 Spectrometer (Bruker, Germany) using KBr pellets. UV–Vis absorption spectra were obtained using a Specord 2450 spectrometer (Shimazu, Japan). The scanning electron microscopic (SEM) images were examined with S-4800 SEM (HITACHI, Japan). TEM micrographs were taken with a JEOL-JEM-2010 (JEOL, Japan) operated at 200 kV.

4. Batch adsorption studies

The adsorption processes were performed by contacting 25 mL of CR dye (C_o: 20, 40, 60, 80, and 100 mg/L) with 10 mg of HNT@Fe_3O_4@LDH in 100 mL flask, agitated on orbital shaker at 30±1°C and 100 rpm. The pH of dye solution was adjusted by using 1M HCl/NaOH prior to the adsorption study. The samples were withdrawn at the fixed time

intervals (0, 5, 10, 15, 20, 30, 60, and 120 min); and the concentration of the CR dye in the samples was analyzed spectrophotometrically at 496 nm. The adsorption isotherms studies were performed in the concentration range of 10–100 mg/L at pH 7, adsorbent dosage of 0.4 g/L, and contact time 48 h. The amount of adsorbed dye was calculated as follows:

$$Q_t = \frac{(C_o - C_t)V}{W} \tag{1}$$

$$Q_e = \frac{(C_o - C_e)V}{W} \tag{2}$$

5. Adsorption kinetics studies

5.1. The pseudo-first-order kinetics model

The pseudo-first-order kinetics model is represented by the following equation [23].

$$\frac{dQ}{dt} = k_1(Q_e - Q_t) \tag{3}$$

Upon integration with initial conditions of $Q_t = 0$ at $t = 0$, and $Q_t = Q_t$ at time, t and upon rearrangement, Eq. (3) transformed as follows:

$$Q_t = Q_e(1 - e^{-k_1 t}) \tag{4}$$

The values of Q_e and k_1 were assessed from the least-square fit of Q_t vs. t at different dyes concentrations.

5.2. The pseudo-second-order kinetics model

This model is given as follows [24]:

$$Q_t = \frac{k_2 Q_e^{\,2} t}{1 + k_2 Q_e t} \tag{5}$$

The values of Q_e and k_2 (g mg^{-1} min^{-1}) were also found from the least-square fit of Q_t vs. t at different solutes concentrations.

5.3. Elovich model

This model is generally expressed as shown in Eq. (6) [25].

$$Q_t = \frac{1}{\beta}\ln(\alpha\beta * t) \tag{6}$$

The constants α and β are related to the rate of the chemisorption and surface coverage, respectively, with their interpretations usually connected to the heterogeneous surfaces [26].

5.4. Intraparticle diffusion model

The intraparticle diffusion model (Eq. (7)) is applied to elucidate the diffusion mechanism during adsorption. The model proposed that the initial diffusion rate is dependent on contact time and surface resistance created by the concentration gradient across the surface.

$$Q_t = K_{id} t^{0.5} + C_i \tag{7}$$

6. Adsorption isotherms

Four common adsorption isotherm models namely, Langmuir, Freundlich, Temkin, and Dubinin–Radushkevich isotherms were applied in this study. The isotherm parameters were obtained by the least-square fit with programme written on MicroMath Scientist software.

6.1. Langmuir isotherms

This model is given as follows [27]:

$$Q_{eq} = \frac{Q_{\max} b C_e}{1 + bC_e} \tag{8}$$

A dimensionless constant separation factor, R_L, which is related to b and initial concentration C_o can be expressed as follows:

$$R_L = \frac{1}{(1 + bC_0)} \tag{9}$$

The value of R_L can be used to evaluate the nature of adsorption obtained from Langmuir isotherm, R_L of zero value indicates irreversible adsorption, the process is favourable when $0 < R_L < 1$, unfavourable when $R_L > 1$ and linear when $R_L = 1$.

6.2. Freundlich isotherm

The Freundlich isotherm is an empirical equation based on sorption on a heterogeneous surface, represented by Eq. (10)[28]:

$$Q_{eq} = K_F C_e^{1/n} \tag{10}$$

where n and K_F are the Freundlich constants related to the intensity and adsorption capacity of the sorbent, respectively.

6.3. Temkin isotherm model

In order to account for the interaction between sorbent and adsorbent, Temkin isotherm model (Eq. (11)) was applied to analyze the equilibrium data. The model proposed that the free energy of sorption is a function of the surface coverage [29].

$$Q_e = \frac{RT}{b_T} \ln a_T C_e \tag{11}$$

where b_T and a_T are the constants related to the heat of adsorption and binding constant at equilibrium corresponding to the maximum binding energy (BE), respectively.

6.4. The Dubinin–Radushkevich isotherm

This model (Eq. (11)) is more general than the Langmuir isotherm and can be used to estimate the heterogeneity of the surface energies as well as classification of adsorption processes into physisorption or chemisorption.

$$Q_e = Q_s e^{-\beta\varepsilon^2} \tag{12}$$

where Q_s is the theoretical saturation capacity (mol g^{-1}), ε is the Polanyi potential given by the relation; ε = ln(1+1/C_e), where C_e (mg/L), R (J mol^{-1} K^{-1}), and T (K) are as previously described. The constant β (mol^2 J^{-2}), is related to the mean free energy E (kJ mol^{-1}) of adsorption per molecule of the adsorbate by $E = (2\beta)^{-0.5}$. If the value of E is less than 8 kJ mol^{-1}, it shows a physisorption process, and if this value is between 8 and 16 kJ mol^{-1}, then the adsorption will be chemical in nature [30,31].

7. Statistical test

Three error functions were applied to confirm the kinetic models fitting, they are sum square error (SSE) function, root-mean-square error (RMSE), and HYBRD (composite fractional error) which are given as follows [9]:

$$\text{SSE} = \sum_{i=1}^{N} (Q_{(\text{exp})} - Q_{(cal)})^2 \tag{13}$$

$$\text{RMSE} = \sqrt{\frac{\sum_{i}^{N} (Q_{(\text{exp})} - Q_{(cal)})^2}{N}} \tag{14}$$

$$\text{HYBRD} = \frac{100}{N-P} \sum_{i}^{N} \frac{(Q_{(\text{exp})} - Q_{(\text{cal})})}{Q_{(\text{exp})}} \tag{15}$$

The lower values of SSE, RMSE, and HYBRD errors and the higher is the value of R^2 indicates the better fitting of the model.

8. Result and discussion

8.1. Characterization of adsorbent

The surface morphologies of halloysite (HNT), magnetite-modified HNT, the intermediate (HNT@Fe_3O_4@AlOOH), and the synthesized HNT@Fe_3O_4@LDH are presented in Figs. 2(a)–(d). The HNT displayed tubular structures with smooth surface, upon modification with magnetic particles (Fig. 2(b)). It is observed that the matrix of the Fe_3O_4 dotted the surface, which could be attributed to the pore volume, large surface area, and presence of functional groups such as OH, has aided the modification. Figs. 2(c) and (d) show the SEM images of HNT@Fe_3O_4@AlOOH and HNT@Fe_3O_4@LDH with fully dispersed AlOOH and LDH on the surface, respectively. The surfaces exhibited a well-dispersed and closed spherical morphology, which is an indication that the outer layer is well coated with the LDH. The energy-dispersive X-ray spectroscopy (EDAX) of the HNT, Fe_3O_4@HNT, HNT@Fe_3O_4@AlOOH, and HNT@Fe_3O_4@LDH, respectively, are shown in Fig. 3. The presence of Fe, Al, Si, and O in the

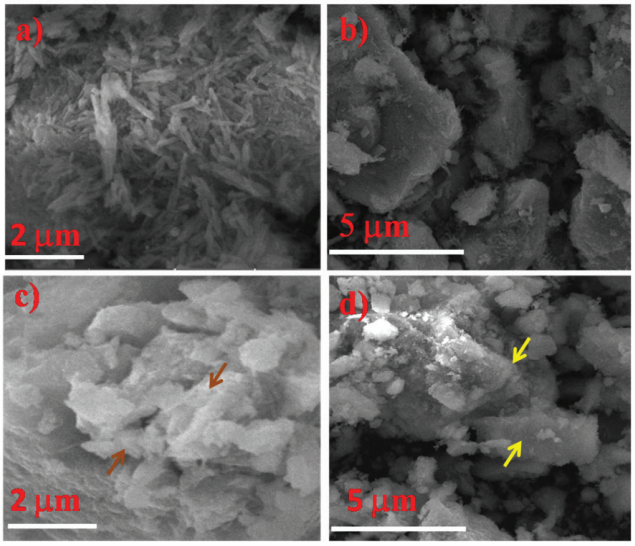

Fig. 2. SEM images of (a) halloysites (HNT), (b) HNT@Fe_3O_4, (c) HNT@Fe_3O_4@AlOOH, and (d) HNT@Fe_3O_4@LDH.

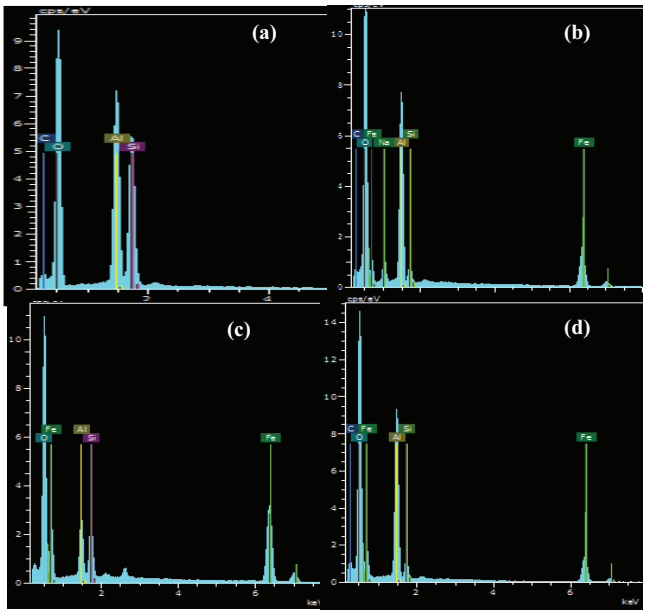

Fig. 3. EDAX analysis of (a) HNT, (b) HNT@Fe_3O_4, (c) HNT@Fe_3O_4@AlOOH, and (d) HNT@Fe_3O_4@LDH.

prepared samples was confirmed. The presence of the C on some of the samples may be attributed to the impurity due to handling and washing with organic solvent.

Figs. 4(a)–(c) present the high-resolution transmission electron microscope (HRTEM) analysis of the HNT, HNT@Fe_3O_4, and HNT@Fe_3O_4@LDH, respectively, with their corresponding selected area electron diffraction (SAED). Fig. 4(a) shows that HNT is a short cylindrical hollow tube with an average length of 700–900 nm, external diameter of 28 nm, and internal diameter of 12 nm. Fig. 4(b) shows that the HNT in magnetic-modified form retained the cylindrical morphology with patches of black Fe_3O_4 deposited on the surface. The SAED pattern exhibits clear-cut hexagonally arranged spots of Fe_3O_4. A well-dispersed crystalline surface of the HNT@Fe_3O_4@LDH is revealed by the HRTEM study (Fig. 4(c)), with flower-like structures of similar shapes and sizes, although the pattern of crystallinity is low when compared with HNT@Fe_3O_4, the arrangement in SAED showed that the sample is a single crystal.

The crystalline structures of the samples were determined by XRD analysis and presented in Fig. 5. The diffraction peaks displayed by HNT were in good accordance with the characteristic peaks of the standard compound Halloysite-7 Å (JCPDS Card No. 29-1487). Upon magnetic growth on its surface, the composite displayed distinct peaks at 2θ values of about 25.13°, 30.33°, 35.67°, 43.56°, 52.11°, 57.14°, and 62.55° as shown in Fig. 4. The XRD pattern of the HNT@Fe_3O_4@AlOOH was alike of the HNT@Fe_3O_4, which showed the crystalline nature of magnetic coating. After the in-situ growth process, the XRD pattern of the resultant HNT@Fe_3O_4@LDH showed the superimposition of reflections of Fe_3O_4 and LDH phases with the planes corresponding to (3 1 1) and (4 4 0) of halloysite at 2θ = 35.67° and 62.55°, which remain conserved despite modifications, indicating the presence of halloysite in the modified samples [32,33].

In order to understand the chemical states of the elements present in the adsorbent, the photoelectron BEs were identified using X-Ray photoelectron spectroscopy (XPS) studies shown in Fig. 6. The survey scan revealed the presence of Fe2p, O1s, Al2p, and Si2p confirming the synthesis of HNT@Fe_3O_4@LDH, the C1s present in the analysis was due to the organic solvent used for washing. The splitting of the deconvoluted lines showed that the elements were present in their various spin states.

The FTIR spectra of the samples are presented in Fig. 7. The fundamental vibration modes of Fe–O, Si–O–Si, and Si–OH groups of the HNT structure are shown by the band at 580, 900–1,030, and 3,300 cm^{-1}, respectively. The band at 1,636 cm^{-1} was allocated to –OH bending vibration of interlayer water [34,35]. The band characteristic to Al–O bond stretching appeared at 651–400 cm^{-1}. The formation of LDH was confirmed due to the presence of bands at 1,382 and 742 cm^{-1}, corresponding to the interlayer CO_3^{2-} interlayer anion of layered Al–LDH. Apart from these vibrations, the bands at 919 and 634 cm^{-1} could be assigned to M–OH and M–O stretching vibrations of LDH. The shift in band position and broadening of peaks was prominent after the modifications owing to the increase in the –OH groups.

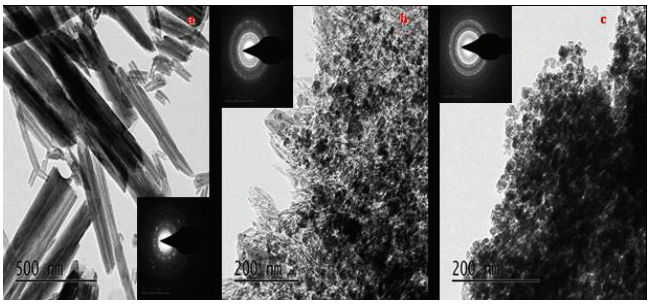

Fig. 4. HRTEM analysis of (a) HNT, (b) HNT@Fe_3O_4, and (c) HNT@Fe_3O_4@LDH.

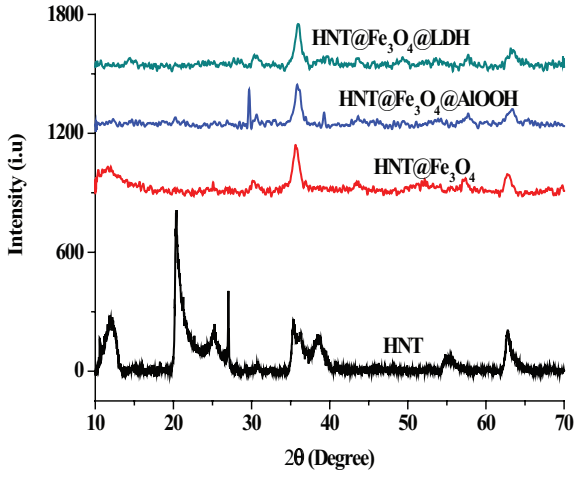

Fig. 5. XRD analysis (a) HNT, (b) HNT@Fe_3O_4, (c)HNT@Fe_3O_4@AlOOH, and (d)HNT@Fe_3O_4@LDH.[TS: Please insert part labels in Figs. 5 and 7.]

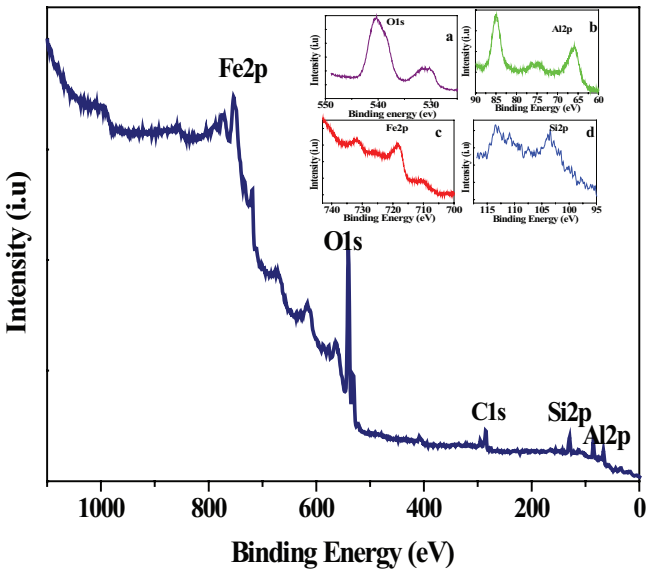

Fig. 6. XPS study of HNT@Fe_3O_4@LDH.

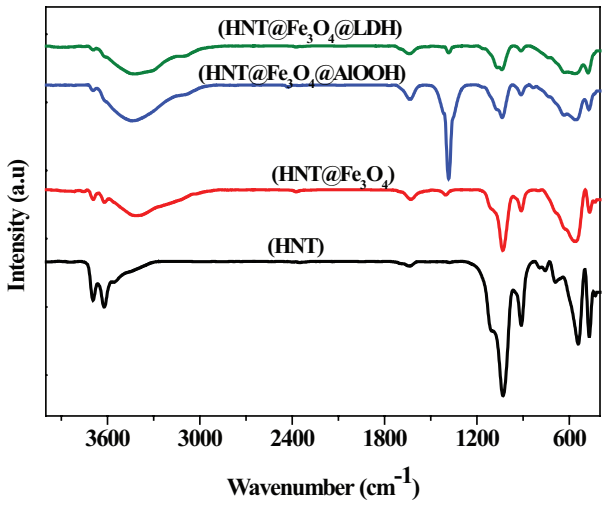

Fig. 7. FTIR Spectra of (a) HNT, (b) HNT@Fe_3O_4, (c)HNT@Fe_3O_4@AlOOH, and (d) HNT@Fe_3O_4@LDH.

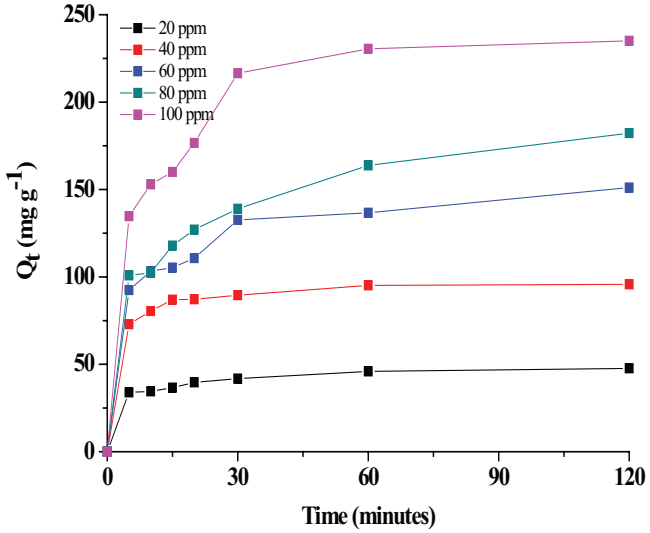

Fig. 8. Effects of contact time and initial concentrations on adsorption of CR dye onto HNT@Fe_3O_4@LDH.

8.2. Effects of contact time and concentrations on the adsorption of CR dye

The effect of time and initial concentrations on the removal of CR dye by HNT@Fe_3O_4@LDH is shown in Fig. 8. The figure showed rapid uptake of the dye in the first 30 min, followed by a gradual increase for the next 120 min after which there was no significant change in the amount adsorbed, inferring a dynamic equilibrium (30–120 min). The adsorption capacity at equilibrium was enhanced from 47.68 to 235.07 mg g^{-1} as the dye concentrations increases from 20 to 100 mg/L.

8.3. Effect of pH on removal efficiency of the adsorbent

The pH of the medium affects the interaction between the adsorbate and adsorbent in aqueous medium [35]. The effect of solution pH on the removal of CR dye by HNT@Fe_3O_4@LDH is given in Fig. 9. The adsorption of CR dye was initially enhanced with increasing the pH, and maximum adsorption was achieved between pH 6 and 7. After pH 7, the adsorption started decreasing. The lower adsorption of CR dye in the acidic medium may probably due to the protonation of the dye molecule and reduction in adsorbent due to part dissolution of the layered materials in an acidic medium [36–38].

8.4. Kinetics and mechanism of adsorption

The knowledge of optimum operational condition is an important criterion in understanding the effectiveness and the adsorption mechanism. Fig. 10 shows the plots of pseudo-first order, second order, Elovich, and intraparticle diffusion models used for the removal of CR dye by HNT@Fe_3O_4@LDH. The parameters for the kinetic models fits are shown in Table 1. At higher concentration, the kinetic data were best fitted with the pseudo-first-order kinetic model. The $Q_{e,calc}$ values were closer to the $Q_{e,exp}$ values for

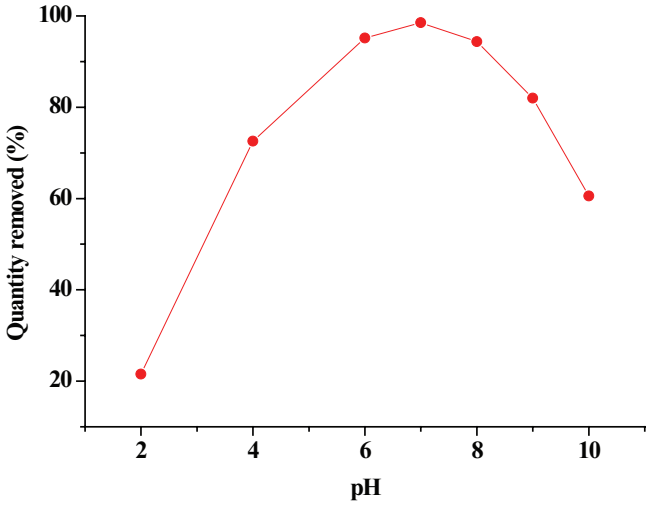

Fig. 9. Effect of pH on the removal of CR dye from aqueous solution.

this model; however, at low concentration the second-order model fitted well, suggesting that chemical interactions between the adsorbent and dye molecule predominate at lower concentration than at higher concentration, the lower average rate also suggested a faster adsorption at beginning which decreases with time. This observation is in agreement with previous studies [39–42]. The Elovich model's parameters indicated that the adsorption rate increased with increasing the initial concentration of the CR dye as indicated by the values of α (adsorption rate) and β (desorption rate), which decreases with increasing the initial concentration which is a sign of physiochemical adsorption of CR dye on toHNT@Fe_3O_4@LDH. The adsorption mechanism was investigated using intraparticle diffusion model. Two diffusion stages were observed for the process; the first stage is rapid and occurs in the first 20 min of the adsorption, while the second, which is a relaxed stage, proceeds until

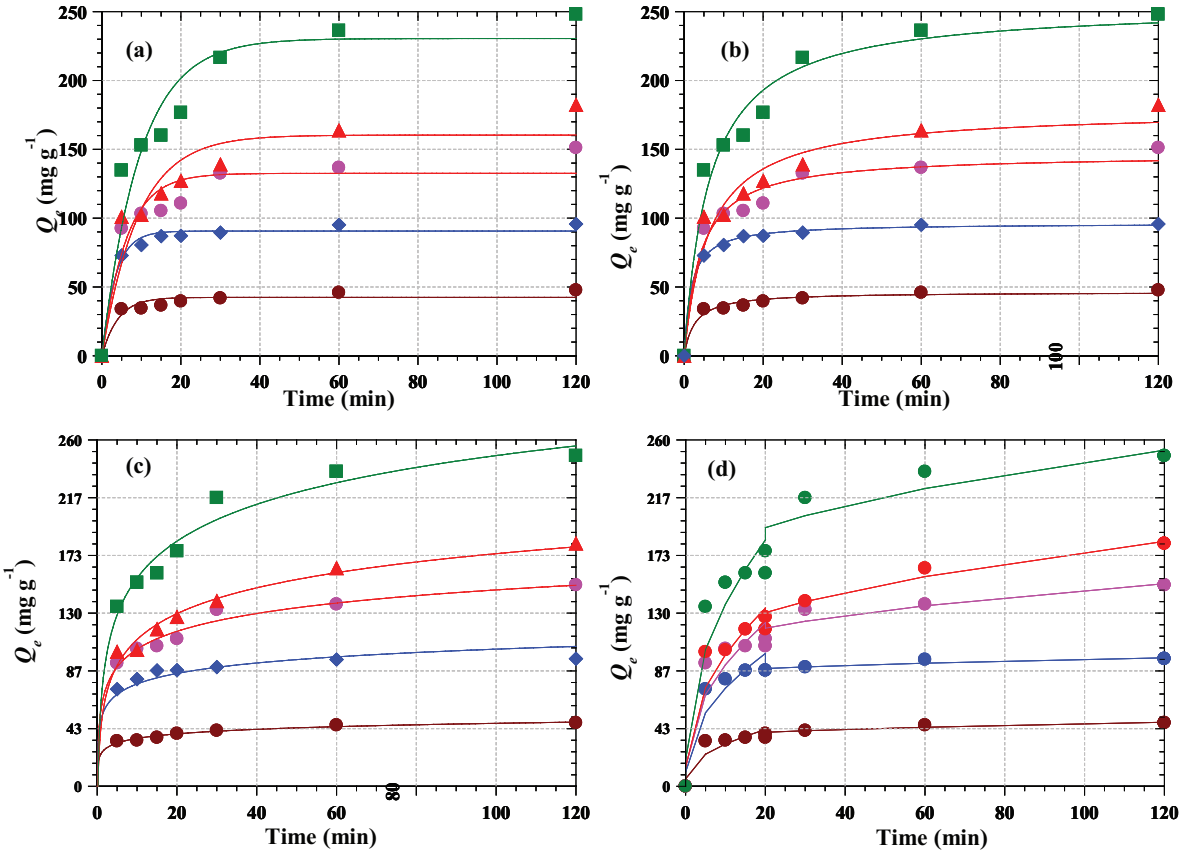

Fig. 10. Kinetic fits for the adsorption of CR dye on HNT@Fe_3O_4@LDH (a) pseudo-first-order model, (b) pseudo-second-order model, (c) Elovich model, and (d) intraparticle diffusion model.

equilibrium. The increase in K_{id} values with increasing the dye concentration could be accredited to the resistance of the surface boundary to the increase driving force with the concentration gradient as these solutes access the available sites on the adsorbent. The values of the intercepts C_i exhibited that the adsorption was initially characterized by the intraparticle diffusion and more significantly by the external mass transfer [4,43].

8.5. Adsorption isotherms

Four different adsorption isotherm models were used for the adsorption of CR dye unto HNT@Fe_3O_4@LDH and shown in Fig. 11. The parameters achieved from the least-square fits of the models are given in Table 2. It is clear from the plots that the adsorption capacity rose momentarily due to the presence of a greater number of active sites which were saturated as the concentration of dyes were increased. The maximum adsorption capacity (Q_{max}) was 225.11 mg g^{-1} by using the Langmuir monolayer equation. The separation factor, R_L obtained for this study was 0.14 while the Freundlich isotherm parameter, n, was 2.49, and these values, respectively, indicated favourable adsorption process. Dubinin–Radushkevich model gave theoretical saturation capacity (Q_s) of 172.85 mg g^{-1}, which was less than the maximum adsorption capacity. The maximum adsorption energies (E) of 0.41 kJ mol^{-1} showed that the process was physisorption in nature. The overall comparison of the fitting of isotherm models based on the R^2 values showed the order Dubinin–Radushkevich > Langmuir > Temkin > Freundlich. When compared with other adsorbents, HNT@Fe_3O_4@LDH performed well with other synthetic and modified adsorbents in removal of CR dye from aqueous solution as depicted in Table 3 [38,44–48].

9. Regeneration study

Reusability of adsorbent is one of the important factors to be considered while selecting adsorbent, because adsorbent with high recyclability will minimize the cost of the adsorption process [49–52]. Desorption studies were performed by the same method as reported earlier [9]. The reusability of HNT@Fe_3O_4@LDH was examined by using regenerated adsorbents for eight successive adsorption–desorption cycles, and the result are presented in Fig. 12. The removal efficiency was obtained nearly 100% for the first four cycles. After the four cycles, there was a slow decrease in the removal efficiency until eighth cycle where the efficiency was achieved 68.03%. This means that surface saturation impaired the efficiency after eight cycles, hence the prepared nanocomposites could be efficiently used for eight times without a significant loss in the removal efficiency [46,47].

Table 1
Kinetic parameters for the adsorption of CR dye by HNT@Fe_3O_4@LDH

Pseudo-first order	C_o (mg/L)	20	40	60	80	100
	$Q_{e,exp}$ (mg g^{-1})	45.93	95.16	136.7	163.76	236.24
	$Q_{e,cal}$ (mg g^{-1})	42.44	90.64	132.54	160.33	230.49
	$k_1 \times 10^2$ (min^{-1})	0.24	0.29	0.16	0.11	0.1
	R^2	0.991	0.998	0.988	0.983	0.988
	%SSE	3.49	4.52	4.16	3.43	5.75
	RMSE	0.39	0.5	0.46	0.38	0.64
	HYBRD	1.17	0.71	0.45	0.31	0.36
Pseudo-second order	$Q_{e,cal}$ (mg g^{-1})	46.362	96.235	146.501	178.439	254.815
	$k_2 \times 10^3$ (g mg^{-1} min^{-1})	8.2	6.02	1.69	0.892	0.612
	R^2	0.997	0.999	0.995	0.993	0.995
	%SSE	0.44	1.08	9.8	14.67	18.57
	RMSE	0.05	0.12	1.09	1.63	2.06
	HYBRD	0.13	0.16	0.96	1.17	1.04
Elovich	$Q_{e,cal}$ (mg g^{-1})	48.183	105.077	150.952	179.735	255.531
	$\alpha \times 10^{-2}$ (mg [g min]$^{-1}$)	7.38	11.5	3.98	1.44	2.01
	β (g mg^{-1})	0.203	0.09	0.052	0.036	0.025
	R^2	0.999	0.997	0.999	0.998	0.998
	%SSE	2.26	9.92	14.25	15.97	19.29
	RMSE	0.25	1.1	1.58	1.77	2.14
	HYBRD	0.67	1.35	1.35	1.27	1.08
Intraparticle diffusion	K_{1d} (mg g^{-1} $min^{-0.5}$)	8.28	19.92	24.15	26.71	36.81
	C_1 (mg g^{-1})	5.6	10.69	14.89	14.41	20.37
	R^2	0.966	0.976	0.97	0.975	0.975
	K_{2d} (mg g^{-1} $min^{-0.5}$)	1.17	1.24	5.15	8.25	8.97
	C_2 (mg g^{-1})	35.31	82.87	95.67	93.52	154.03
	R^2	0.999	0.999	0.998	0.999	0.997

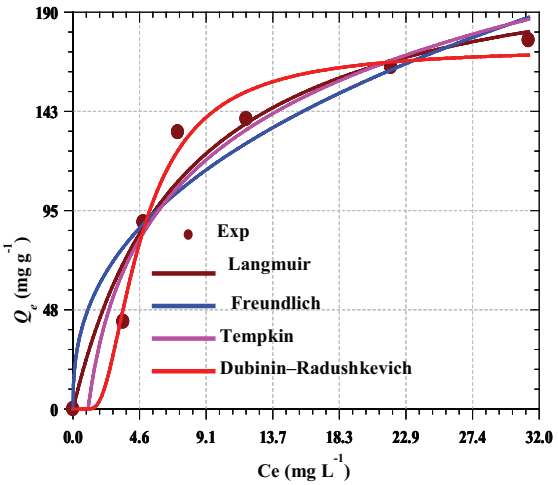

Fig. 11. Isotherm models for the adsorption of CR dye onto HNT@Fe_3O_4@LDH.

Table 2
Isotherm parameters for CR dye adsorption using HNT@Fe_3O_4@LDH

Isotherms	Parameter	
Langmuir	Q_{max} (mg g^{-1})	225.11
	b (L mg^{-1})	0.13
	R_L	0.14
	R^2	0.987
Freundlich	K_F ([mol g^{-1}][mol L^{-1})$^{-1/n}$)	47.1
	n	2.49
	R^2	0.978
Temkin	a_T (L mg^{-1})	46.02
	b_T	0.97
	R^2	0.986
Dubinin–Radushkevich	Q_s (mg g^{-1})	172.85
	$\beta \times 10^6$ (mol J^{-1})^2	3.11
	E (kJ mol^{-1})	0.41
	R^2	0.997

Table 3
Comparison of monolayer adsorption capacity using different adsorbents

Adsorbent	Q_e (mg g^{-1})	Reference
Cellulose/Fe_3O_4/activated carbon composite	66.0	38
Cross-linked cationic polyamine folic acid composites	204.1	44
Fe_3O_4@graphene composite	33.66	45
Kaolin (clay materials)	5.44	46
Maghemite nanoparticles	20.0	47
Magnetic core–manganese oxide shell	42.0	48
PPy–PANI NFs	50.50	49
HNT@Fe_3O_4@LDH	225.11	This study

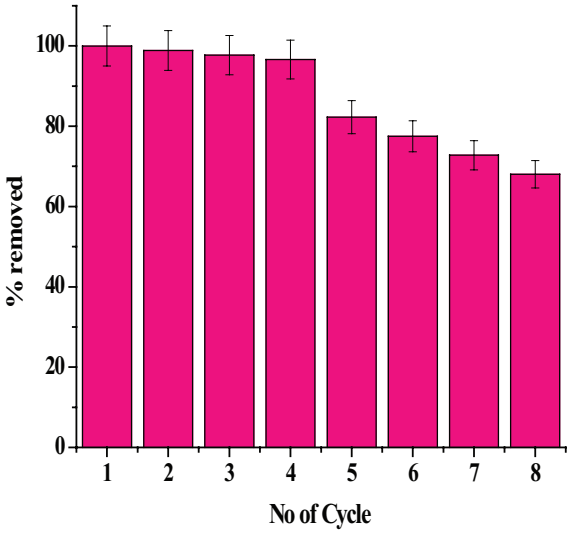

Fig. 12. CR dye removal efficiency of regenerated HNT@Fe_3O_4@LDH.

10. Conclusion

HNT@Fe_3O_4@LDH was successfully synthesized, characterized, and subsequently used for the removal of CR dye from aqueous medium. The adsorption process was affected with the change of contact time, initial pollutant concentration, and pH of the solution. The pseudo-first-order kinetic model was found to be the best-fit model to describe the adsorption process. The maximum monolayer adsorption capacity was found to be 225.11 mg g^{-1} using the Langmuir equation. It is, therefore, apparent that HNT@Fe_3O_4@LDH is a potential adsorbent for the adsorptive removal of CR dye from aqueous medium.

Acknowledgment

The authors are thankful to the CSIR-Central Electro Chemical Research Institute, India, for providing research facilities.

References

[1] E. Daneshvar, A. Vazirzadeh, A. Niazi, M. Kousha, M. Naushad, A. Bhatnagar, Desorption of Methylene blue dye from brown macroalga: effects of operating parameters, isotherm study and kinetic modeling, J. Cleaner Prod., 152 (2017) 443–453.
[2] G. Sharma, M. Naushad, A. Kumar, S. Rana, S. Shweta, A. Bhatnagar, F.J. Stadler, A.A. Ghfar, M.R. Khan, Efficient removal of coomassie brilliant blue R-250 dye using starch/poly(alginic acid-*cl*-acrylamide) nanohydrogel, Proc. Safe Environ. Prot., 109 (2017) 301–310.
[3] K.L. Han, T.T. Tjoon, H.I. Mahamad, A. Anees, T.C. Hui, Adsorption and removal of zinc (II) from aqueous solution using powdered fish bones, APCBEE Procedia, 1 (2012) 96–102.
[4] A.I. Adeogun, B.R. Babu, One-step synthesized calcium phosphate-based material for the removal of alizarin S dye from aqueous solutions: isothermal, kinetics, and thermodynamics studies, Appl. Nanosci., 6 (2015) 1–3.
[5] A.A. Alqadami, M. Naushad, Z.A. Alothman, T. Ahamad, Adsorptive performance of MOF nanocomposite for methylene blue and malachite green dyes: kinetics, isotherm and mechanism, J. Environ. Manage., 223 (2018) 29–36.
[6] A.A. Alqadami, M. Naushad, M.A. Abdalla, T. Ahamad, Z.A. ALOthman, S.M. Alshehri, A.A. Ghfar, Efficient removal of toxic metal ions from wastewater using a recyclable nanocomposite: a study of adsorption parameters and interaction mechanism, J. Cleaner Prod., 156 (2017) 426–436.
[7] A.L. Ahmad, W.A. Harris, Syafiie, O.B. Seng, Removal of dye from wastewater of textile industry using membrane technology, J. Teknol., 36 (2002) 31–44.
[8] M. Naushad, Z.A. ALOthman, M. Islam, Adsorption of cadmium ion using a new composite cation-exchanger polyaniline Sn(IV) silicate: kinetics, thermodynamic and isotherm studies, Int. J. Environ. Sci. Technol., 10 (2013) 567–578.
[9] S. Vahidhabanu, D. Karuppasamy, A.I. Adeogun, B. Ramesh Babu, Impregnation of zinc oxide modified clay over alginate beads: a novel material for the effective removal of congo red from wastewater, RSC Adv., 7 (2017) 5669.
[10] S. Vahidhabanu, A. AbideenIdowu, D. Karuppasamy, B. Ramesh Babu, M. Vineetha, Microwave initiated facile formation of sepiolite-poly (dimethylsiloxane) nanohybrid for effective removal of congo red dye from aqueous solution, ACS Sustainable Chem. Eng., 5 (2017) 10361–10370.
[11] A.A. Alqadami, M. Naushad, M.A Abdalla, M.R. Khan, Z.A. ALOthman, Adsorptive removal of toxic dye using Fe_3O_4–TSC nanocomposite: equilibrium, kinetic, and thermodynamic studies, J. Chem. Eng. Data, 61 (2016) 3806–3813.
[12] M. Naushad, Z.A. ALOthman, M.R. Awual, M.M. Alam, G.E. Eldesoky, Adsorption kinetics, isotherms and thermodynamic studies for the adsorption of Pb^{2+} and Hg^{2+} metal ions from aqueous medium using Ti(IV) iodovanadatecation exchanger, Ionics, 21 (2015) 2237–2245.
[13] M. Naushad, T. Ahamad, B.M. Al-Maswari, A.A. Alqadami, S.M. Alshehri, Nickel ferrite bearing nitrogen-doped mesoporous carbon as efficient adsorbent for the removal of highly toxic metal ion from aqueous medium, Chem. Eng. J., 330 (2017) 1351–1360.
[14] S.I. Siddiqui, S.A. Chaudhry, *Nigella sativa* plant based nanocomposite-$MnFe_2O_4$/BC: a non-toxic, antibacterial material for water purification application, J. Cleaner Prod., 200 (2018) 996–1008.
[15] P. Calcagnile, F. Despina, S.B. Ilker, C.A. George, M. Luigi, P.C. Davide, C. Roberto, A. Athanassia u, Magnetically driven floating foams for the removal of oil contaminants from water, ACS Nano., 6 (2012) 5413–5419.

[16] S. Mellouk, S. Cherifi, M. Sassi, K. Marouf-Khelifa, A. Bengueddach, J. Schott, A. Khelifa, Intercalation of halloysite from Djebel Debagh (Algeria) and adsorption of copper ions, Appl. Clay Sci., 44 (2009) 230–236.
[17] G. Kiani, High removal capacity of silver ions from aqueous solution onto halloysite nanotubes, Appl. Clay Sci., 90 (2014) 159–164.
[18] Y. Zhao, E. Abdullayev, A. Vasiliev, Y. Lvov, Halloysite nanotubule clay for efficient water purification, J. Colloid Interface Sci., 406 (2013) 121–129.
[19] G. Cavallaro, G. Lazzara, S. Milioto, F. Parisi, V. Sanzillo, Modified halloysite nanotubes: nanoarchitectures for enhancing the capture of oils from vapor and liquid phases, ACS Appl. Mater. Interfaces, 6 (2014) 606–612.
[20] S. Mandal, S. Mayadevi, Adsorption of fluoride ions by Zn−Al layered double hydroxides, Appl. Clay Sci., 40 (2008) 54.
[21] S. Mingfei, N. Fanyu, Z. Jingwen, W. Min, G.E. David, D. Xue, Preparation of Fe_3O_4@SiO_2@layered double hydroxide core–shell microspheres for magnetic separation of proteins, J. Am. Chem. Soc.,134 (2012) 1071−1077.
[22] F. Granados-Correa, J. Jimenez-Becerril, Chromium (VI) adsorption on boehmite, J. Hazard. Mater., 162 (2009) 1178–1174.
[23] G.H. Lin, D.J. Brusick, Mutagenicity studies on two triphenylmethane dyes, Bromophenol blue and tetrabromophenol blue, J. Appl. Toxicol., 12 (1992) 267–274.
[24] Y.S. Ho, G. McKay, The kinetics of sorption of basic dyes from aqueous solution by sphagnum moss peat, Can. J. Chem. Eng., 76 (1998) 822–827.
[25] S.H. Chien, W.R. Clayton, Application of Elovich equation to the kinetics of phosphate release and sorption in soils, Soil Sci. Soc. Am. J., 44 (1980) 265–268.
[26] Y. Liu, L. Shen, From Langmuir kinetics to first- and second-order rate equations for adsorption, Langmuir, 24 (2008) 11625–11630.
[27] I. Langmuir, The adsorption of gases on plane surfaces of glass, mica, and platinum, J. Am. Chem. Soc.,40 (1918) 1361–1403.
[28] H.M.F. Freundlich, Over the adsorption in solution, J. Phys. Chem., 57 (1906) 385–470.
[29] M.O. Nkiko, A.I. Adeogun, N.A. Babarinde, O.J. Sharaibi, Isothermal, kinetics and thermodynamics studies of the biosorption of Pb(II) ion from aqueous solution using the scale of croaker fish (Genyonemuslineatus), J. Water Reuse Desal., 3 (2013) 239–248.
[30] S. Kundu, A.K. Gupta, Arsenic adsorption onto iron oxide-coated cement (IOCC), regression analysis of equilibrium data with several isotherm models and their optimization, Chem. Eng. J., 122 (2006) 93–106.
[31] A.I. Adeogun, M.A. Idowu, A.E. Ofudje, S.O. Kareem, S.A. Ahmed, Comparative biosorption of Mn(II) and Pb(II) ions on raw and oxalic acid modified maize husk: kinetic, thermodynamic and isothermal studies, Appl. Water Sci., 3 (2013) 167–179.
[32] L. Li, F. Wang, Y. Lv, J. Liu, D. Zhang, Z. Shao, Halloysite nanotubes and Fe_3O_4 nanoparticles enhanced adsorption removal of heavy metal using electrospun membranes, Appl. Clay Sci., 161 (2018) 225–234.
[33] T. Tsoufis, F. Katsaros, B.J. Kooi, E. Bletsa, S. Papageorgiou, Y. Deligiannakis, I. Panagiotopoulos, Halloysite nanotube-magnetic iron oxide nanoparticle hybrids for the rapid catalytic decomposition of pentachlorophenol, Chem. Eng. J., 313 (2017) 466–474.
[34] S. Zhong, C. Zhou, X. Zhang, H. Zhou, H. Li, X. Zhu, Y. Wang, A novel molecularly imprinted material based on magnetic halloysite nanotubes for rapid enrichment of 2,4-dichlorophenoxyacetic acid in water, J. Hazard. Mater., 276 (2014) 58–65.
[35] K. Zhu, Y. Duan, F. Wang, P. Gao,H. Jia,C. Ma, C.Wang, Silane-modified halloysite/Fe_3O_4 nanocomposites: simultaneous removal of Cr(VI) and Sb(V) and positive effects of Cr(VI) on Sb(V) adsorption, Chem. Eng. J., 311 (2017) 236–246.
[36] S.I. Siddiqui, S.A. Chaudhry, Iron oxide and its modified forms as an adsorbent for arsenic removal: a comprehensive recent advancement, Proc. Safe Environ. Prot., 111 (2017) 592–626.
[37] G. Chao, Y. Xin-Yao, L. Tao, J. Yong, S. Bai, L. Jin-Huai, H. Xing-Jiu, Millimeter-sized Mg–Al-LDH nanoflake impregnated magnetic alginate beads (LDH-n-MABs): a novel bio-based sorbent for the removal of fluoride in water, J. Mater. Chem. A, 2 (2014) 2119–2128.
[38] H.Y. Zhu, Y.Q. Fu, R. Jiang, L. Xiao, G.-M. Zeng, S.-L. Zhao, Y. Wang, Show more adsorption removal of Congo red onto magnetic cellulose/Fe_3O_4/activated carbon composite: equilibrium, kinetic and thermodynamic studies, Chem. Eng. J., 173 (2011) 494–502.
[39] G. Ren, X. Wang, P. Huang, B. Zhong, Z. Zhang, L. Yang, X. Yang, Chromium (VI) adsorption from wastewater using porous magnetite nanoparticles prepared from titanium residue by a novel solid-phase reduction method, Sci. Total Environ., 607–608 (2017) 900–910.
[40] S. Azizian, Kinetic models of sorption: a theoretical analysis, J. Colloid Interface Sci., 276 (2004) 47–52.
[41] Y.-S. Ho, G. McKay, The kinetics of sorption of divalent metal ions onto sphagnum moss peat, Water Res., 34 (2000) 735–742.
[42] S.I. Siddiqui, S.A. Chaudhry, Removal of arsenic from water through adsorption onto metal oxide-coated material, Mater. Res. Found., 15 (2017) 227–276.
[43] S.I. Siddiqui, G. Rathi, S.A. Chaudhry, Acid washed black cumin seed powder preparation for adsorption of methylene blue dye from aqueous solution: thermodynamic, kinetic and isotherm studies, J. Mol. Liq., 264 (2018) 275–284.
[44] M.K. Nayunigari, R. Das, A. Maity, S. Agarwal, V.K. Gupta, Folic acid modified cross-linked cationic polymer: synthesis, characterization and application of the removal of Congo red dye from aqueous medium, J. Mol. Liq., 227 (2017) 87–97.
[45] Y. Yao, S. Miao, S. Liu, L.P. Ma, H. Sun, S. Wang, Synthesis, characterization, and adsorption properties of magnetic Fe_3O_4@ graphene nanocomposite, Chem. Eng. J., 184 (2012) 326–332.
[46] V. Vimonses, S. Lei, B. Jin, C.W. Chow, C. Saint, Kinetic study and equilibrium isotherm analysis of Congo red adsorption by clay materials, Chem. Eng. J., 148 (2009) 354–364.
[47] A. Afkhami, R. Moosavi, Adsorptive removal of Congo red, a carcinogenic textile dye, from aqueous solutions by maghemite nanoparticles, J. Hazard. Mater., 174 (2010) 398–403.
[48] Y. Zhai, J. Zhai, M. Zhou, S. Dong, Ordered magnetic core manganese oxide shell nanostructures and their application in water treatment, J. Mater. Chem., 19 (2009) 7030–7035.
[49] Mu. Naushad, S. Vasudeva, G. Sharma, A. Kumar, Z.A. ALOthman, Adsorption kinetics, isotherms and thermodynamic studies for Hg^{2+} adsorption from aqueous medium using alizarin red-S loaded amberlite IRA-400 resin, Desal. Wat. Treat., 57 (2016) 18551–18559.
[50] A.A. Alqadami, M. Naushad, Z.A. ALOthman, A.A. Ghfar, Novel metal–organic framework (MOF) based composite material for the sequestration of U(VI) and Th(IV) metal ions from aqueous environment, ACS Appl. Mater. Int., 9 (2017) 36026–36037.
[51] M. Naushad, T. Ahamad, G. Sharma, M.M. Alam, Z.A. ALOthman, S.M. Alshehri, A.A. Ghfar, Synthesis and characterization of a new starch/SnO_2 nanocomposite for efficient adsorption of toxic Hg^{2+} metal ion, Chem. Eng. J., 300 (2016) 306–316.
[52] Z. Li, X. Tang, K. Liu, J. Huang, Q. Peng, M. Ao, Z. Huang, Fabrication of novel sandwich nanocomposite as an efficient and regenerable adsorbent for methylene blue and Pb(II) ion removal, J. Environ. Manage., 218 (2018) 363–373.